Aerosol Science and Technology

ISSN: (Print) (Online) Journal homepage: www.tandfonline.com/journals/uast20

Dust resuspension from the splash of a falling powder: A numerical aerodynamic simulation of a pellet falling onto a powder monolayer

Leonid A. Turkevich, Hongyu Chen & Milind A. Jog

To cite this article: Leonid A. Turkevich, Hongyu Chen & Milind A. Jog (2025) Dust resuspension from the splash of a falling powder: A numerical aerodynamic simulation of a pellet falling onto a powder monolayer, Aerosol Science and Technology, 59:1, 49-65, DOI: 10.1080/02786826.2024.2417976

To link to this article: https://doi.org/10.1080/02786826.2024.2417976

AEROSOL SCIENCE AND TECHNOLOGY
2025, VOL. 59, NO. 1, 49–65
https://doi.org/10.1080/02786826.2024.2417976

Dust resuspension from the splash of a falling powder: A numerical aerodynamic simulation of a pellet falling onto a powder monolayer

Leonid A. Turkevich[a], Hongyu Chen[b], and Milind A. Jog[b]

[a]Division of Field Studies & Engineering (DFSE), National Institute for Occupational Safety & Health (NIOSH), The Centers for Disease Control & Prevention (CDC), Alice Hamilton Laboratory, Cincinnati, Ohio, USA; [b]Thermal Fluids & Thermal Processing Lab, Mechanical & Materials Engineering, University of Cincinnati, Cincinnati, Ohio, USA

ABSTRACT

A falling powder can generate a dust cloud from its interaction with the ambient air and from its splash onto a substrate. This article reports the results of a numerical simulation study, which attempts to model this second process. We argue that the dust cloud arises from the aerodynamic resuspension of previously deposited small particles. The agglomerated falling powder is modeled as a falling pellet disk impacting a surface covered with a monolayer of previously deposited particles. The Reynolds number of the air flow in the vicinity of the impacting pellet is Re $\sim$ 1860, so the air flow is modeled as laminar and incompressible. The dust particles are incorporated *via* a Lagrangian multiphase treatment. The sudden deceleration of the disk sheds an aerodynamic vortex, which suspends particles from the monolayer. Characteristics of the dust cloud (average and maximum height and radius) are tracked; these are conveniently summarized by following the trajectory of the dust cloud centroid. The probability of aerosolization decreases with distance from the impacted pellet. The centroid trajectory is studied as a function of dust particle size. The model is relatively insensitive to disk radius and thickness. More realistic modeling of dust clouds generated by the splash of falling powders will require a statistical analysis of aggregate size and location, as well as the inclusion of interparticle and particle-surface interactions.

GRAPHICAL ABSTRACT

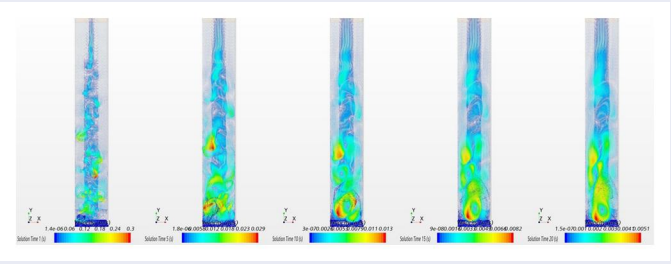

ARTICLE HISTORY
Received 14 March 2024
Accepted 22 July 2024

EDITOR
Johnathan P. Reid

1. Introduction

1.1. Motivation and outline

We are interested in sources of inhaled particulate exposure; a ubiquitous source is the dust generated by falling powders. There are two mechanisms for dust generation: aerosol that results intrinsically from the falling powder stream; aerosol that results from the "splash" of the powder as it impacts a surface. Modeling the first process is the subject of a forthcoming article. The current article presents the results of a simple model for this second "splash" process. We argue that dust generated by this "splash" process derives from the aerodynamic resuspension of particles previously deposited on the surface; the aerodynamic forces are associated with the decelerating powder agglomerates.

CONTACT Leonid A. Turkevich LLT0@cdc.gov Division of Field Studies & Engineering (DFSE), National Institute for Occupational Safety & Health (NIOSH), The Centers for Disease Control & Prevention (CDC), Alice Hamilton Laboratory, 1090 Tusculum Avenue, Cincinnati, OH 45226, USA.

Supplemental data for this article is available online at https://doi.org/10.1080/02786826.2024.2417976

Resuspension has been actively studied for some time—for a review, see Ferro (2022). Most resuspension studies focus on overcoming the adhesive forces binding the particles to the substrate (John 1995). However, Cleaver and Yates (1973) investigated the role of turbulent flow at the surface in particle detachment. Our interest is in the bulk aerodynamics leading to detachment and in the subsequent evolution of the aerosol dust cloud.

We first review (Section 1.2) real world sources of dust exposure and its measurement; we then focus (Section 1.3) on falling powders and distinguish (Section 1.4) the splash process; Section 1.5 defines our model of a descending pellet (representing an agglomerate) impacting a surface covered with a monolayer of primary particles. Section 2 summarizes our numerical methods. Section 3 discusses our results. Section 4 places our results in the context of the previous work by Shields on the (hydrodynamic) resuspension (of sediment) due to turbulent parallel flow.

1.2. Dust

Industrial powder handling represents a primary source of dust. Processes like powder spilling (Sutter, Johnston, and Mishima 1982), pouring (Heitbrink, Baron, and Willeke 1992), and conveying (Baker et al. 1986; Cheng 1973) can all lead to the generation of dust in occupational environments. Grinding and milling operations can also contribute to dust generation (Pensis et al. 2010). Conveyor transferring and the loading and unloading of bulk materials, like ore and agricultural products, can lead to dust generation (Chen et al. 2012; Shaw et al. 1998).

Dust can adversely affect human health. Silicosis, asbestosis, lung cancer, and heart disease are all related to dust exposure (Donaldson and Seaton 2012). Size and surface chemistry contribute to the toxicity of inhaled powders (Duffin et al. 2002, 2007). The health hazards associated with exposure to nanoparticles are of current interest (Trout and Schulte 2010). Increased production and use of nanomaterials presage increased occupational exposure to dust from these materials (Evans et al. 2010; Kuhlbusch et al. 2011; Peters et al. 2008).

A free-falling powder is a common source of airborne dust, often occurring during a materials transfer process, or an accidental spill. Manual powder handling operations, such as silo or bag filling from a hopper, bag emptying, powder weigh-out, and powder transfer from a conveyor, all involve free-falling powders. The mechanisms of dust generation from free falling powders are not well understood.

Dustiness quantifies the ability of a finely divided solid (a powder) to become airborne as a dust aerosol when the powder is subjected to a mechanical or aerodynamical stimulus (Liden 2006; Plinke et al. 1995). Various dustiness measurement methods have been developed (BOHS 1985; Hamelmann and Schmidt 2003, 2004, 2005). Three types of dustiness testing methods are commonly used: the rotating drum method, the free-falling powder method, and the Venturi method. For a comprehensive review of dustiness test methods, see Evans (2024). Field evaluations of worker dust exposure do not always correlate with dustiness test results (Brouwer et al. 2006; Heitbrink, Todd, and Fischbach 1989; Heitbrink et al. 1990; Ribalta et al. 2019).

Several historical dustiness test configurations utilize the falling powder geometry. Falling powder test systems can be of the single drop type, where a powder sample is dropped as a single bolus and impacts onto a solid surface, or the continuous falling type, where a continuous stream of powder winnows down a test chamber. Continuous falling methods tend to be more consistent than single drop methods (BOHS 1988); nonetheless, the majority of falling powder configurations are single-drop type.

1.3. Falling powder dustiness tests

Powell and Russell (1933) described a *single-drop* test with passive dust sampling to quantify coal and coke dust release; ASTM D547-41 (1980) standardized this test method. BOHS (1985) described a scaled down version with active particle samplers. Lundgren (1986) and Lundgren and Rangaraj (1986) similarly used active sampling. In a classical study, Andreasen, Hofman-Bang, and Rasmussen (1939) used the single drop technique to compare the dustiness of a wide range of materials against a lycopodium reference standard.

The Roaches Dust Particle Apparatus was developed to test dyestuffs (Berger-Schuun et al. 1989) and was later evaluated by Lyons and Mark (1992). A single bolus of test powder falls into a quiescent chamber and impacts onto a base surface. In the Palas Dustview II version, the aerosol is optically monitored. O'Shaughnessy, Kang, and Ellickson (2012) described a low mass variant of this test.

Burdett et al. (2000) describe a single drop test configuration with optical extinction detection,

standardized as DIN 55992-2 (1999). The test powder falls down a column; a gentle cross flow of air transports the dusty aerosol to size selective particle collection foams (CEN 1993; ISO 1995; Vincent et al. 1999). Splashing of the falling test powder from the impaction plate introduces variability. The Carr dispersibility test (ASTM 2021) measures the aerosolized dust as that gravimetric fraction of the dropped bolus that does not deposit on a collection surface at the base of the chamber.

Wells and Alexander (1978) described a *continuous pour* configuration. Dust is measured from air drawn horizontally across the falling powder. In the MRI (Midwest Research Institute) pouring device (Cowherd, Grelinger, and Wong 1989), a powder falls onto a powder covered receiving surface; a rotating, vibrating stainless-steel sample cup ensures a continuous stream of powder. EN15051-3 (CEN 2013) and EN17199-3 (CEN 2019) standardize a continuously metered falling powder test, performed against a slow countercurrent of upward moving air (Dahmann, Hartfiel, and Mocklinghoff 1997).

Computational Fluid Dynamics (CFD) has previously been used to study various dustiness testers. Dubey, Ghia, and Turkevich (2017) used CFD to investigate injection and sampling in the Venturi dustiness tester (VDT). The aerosolization within the VDT injection tube has also been investigated with CFD (Palakurthi 2017; Palakurthi, Ghia, and Turkevich 2017, 2022; Sharma 2021; Sharma, Ghia, and Turkevich 2020a, 2020b). Chen et al. (2021) and Chen, Jog, and Turkevich (2023) used CFD to investigate dust behavior in the standard (EN15051-2) and high-speed (Heubach) rotating drums. Schulz et al. (2019) used CFD-DEM to investigate the dustiness of bulk material handling in high-speed rotation drums as well as in the Palas Dust View apparatus. Chen et al. (2023) used CFD to study surface dust aerosolization by a turbulent parallel jet. Ansart et al. (2009, 2011) and Ansart, de Ryck, and Dodds (2009) used an Euler-Euler multiphase model to investigate the intrinsic dust generation from a continuous falling powder.

1.4. The splash process

Heitbrink (1990) and coworkers (Heitbrink, Baron, and Willeke 1992) emphasized the additional dust generated by the "splash" of the powder from the substrate. A single bolus of powder fell either onto a flat plate or into a water-filled beaker. The difference in aerosol concentration caused by changing the impact surface was assumed to be the aerosol caused by processes that occur when the powder hits the flat plate. Two fine aluminum oxide powders were studied. Comparable contributions to the aerosol were generated from the powder as it falls and from the impact. The impact aerosol was enhanced in ultra-fines compared with the aerosol aerodynamically generated from the falling powder (Heitbrink 1990).

The Ibaseta-Biscans experiment (2007) was inspired by the MRI test (Cowherd et al. 1989). The powder was released from an invertible beaker; aerosol concentration and size distributions were measured at various heights. Two nanostructured powders were studied: anatase TiO_2 and fumed SiO_2. Aerosol was produced by two mechanisms: dust generation from the falling powder and dust generation after impact on the chamber floor. Most of the aerosol was generated during the impact against the solid surface and then was upwardly convected. Once the aerosol was uniform in the chamber, the aerosol concentration decreased homogeneously *via* settling. We have visualized the second "splash" process in our laboratory.

A nominally 3 μm calcium carbonate powder (Dust Chaser Fluorescent Leak Detector Powder from W. H. Kingsmill, Ltd., Burlington, ON, Canada: 75% calcium carbonate, 25% resin: 1,3-isobenzofurandiole polymer with 2,2-bis(hydroxymethyl)-1,3 propanediol to incorporate pink fluorescent pigment) is poured from a glass beaker, at a height of ~0.5 m, onto a Plexiglas tray (with rim). The pouring powder is illuminated with UV light (100 LED Scorpion Master with peak $\lambda = 390$ nm); the pouring process is recorded with a Camcorder (Hitachi DZ-BD10HA) at 30 fps. The powder stream is intermittent (rather than continuous), reflecting cohesive agglomeration of the powder; the falling aggregates appear brightly illuminated (Figure 1a).

After 0.3 s, a fainter dust cloud (presumably consisting of smaller particles) rises from, and bounded by, the rim of, the Plexiglas tray (Figure 1b). The particle size distribution (SEM analysis conducted by Maxxam, Bureau Veritas, Kennesaw, GA) of the original powder contains a significant submicron fraction (33.2% with $l < 1$ μm) in addition to the larger particles (41.2% with $1\ \mu m < l < 2\ \mu m$; 15.6% with $2\ \mu m < l < 3\ \mu m$; 6.3% with $3\ \mu m < l < 5\ \mu m$; 2.9% with $5\ \mu m < l < 10\ \mu m$; 0.8% with $l > 10$ μm).

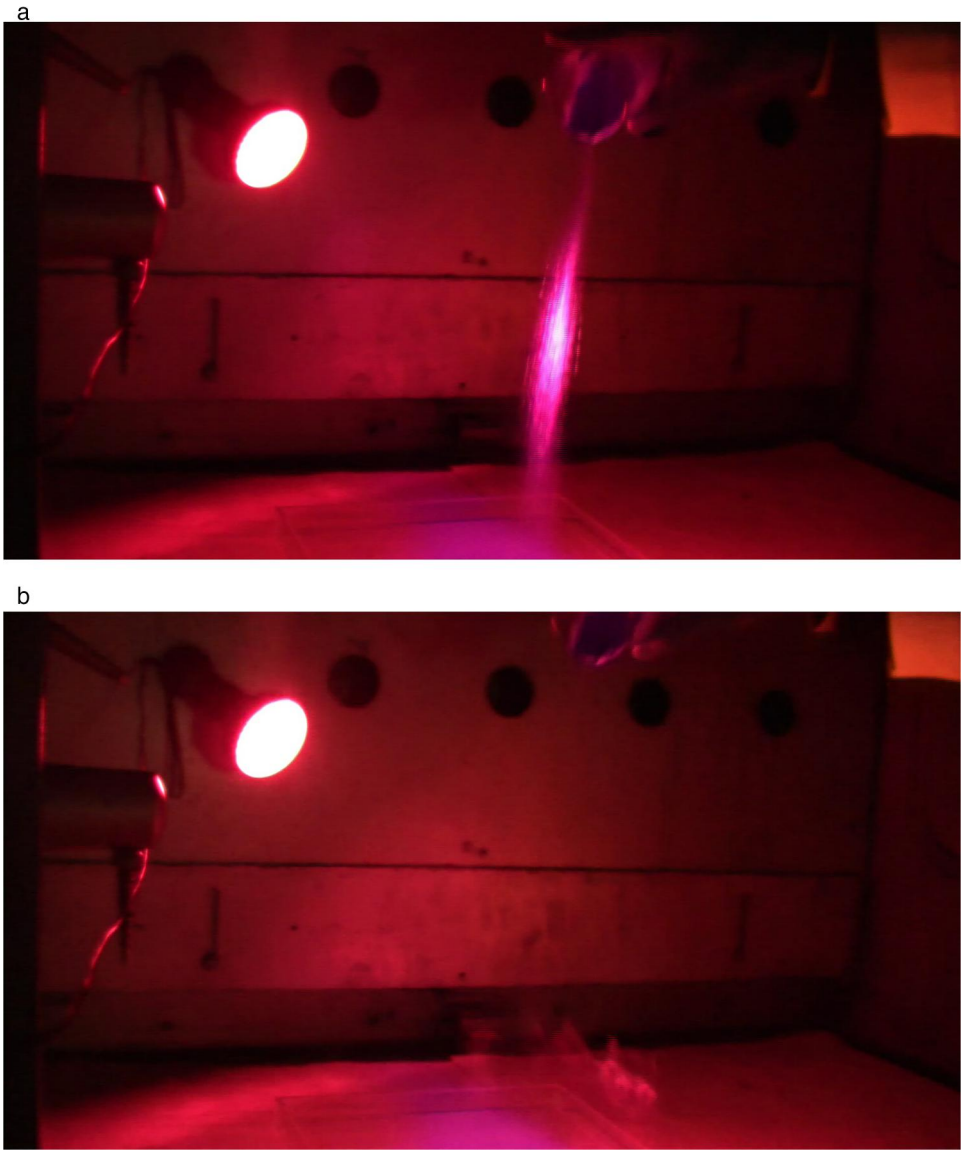

Figure 1. Photographs of falling powder: (a) $t = 0$: stream of falling aggregates; (b) $t = 0.3$ s: dust cloud resulting from the splash process.

2. Methods

2.1. Modeling a falling powder

A falling powder generates dust *via* two processes: (a) dust generation directly by the falling powder (air-particle interaction—upper part of figure), and (b) dust generation resulting from powder agglomerates impacting the bottom surface (lower part of figure) (Figure 2).

In the first process, the falling powder entrains flow in the surrounding air (CEN 2013). The velocity gradient, between the falling powder and the quiescent air, transfers kinetic energy from the powder into air motion. The resultant air flow is complicated and is the subject of a future study.

In the second process, when agglomerated powder impacts the bottom surface, the accompanying air flow resuspends individual particles that had previously been deposited on the surface (Andreasen, Hofman-Bang, and Rasmussen 1939; BOHS 1985; Cawley and Leith 1993; Cowherd, Grelinger, and Wong 1989; Hammond 1980; Heitbrink, Baron, and Willeke 1992; Plinke, Leith, Boundy, et al. 1994; Plinke, Maus, and Leith 1992; Plinke et al. 1991). The present article reports the results of simulations of this second process. Plinke, Leith, Goodman, et al. (1994) studied the impaction force of falling powder agglomerates on the substrate.

Individual primary particles falling onto the bottom of the chamber do not contribute to the splash aerosol; they merely sediment at their Stokes terminal velocity. Large particle agglomerates falling to the bottom, or the collective motion of the dense particle

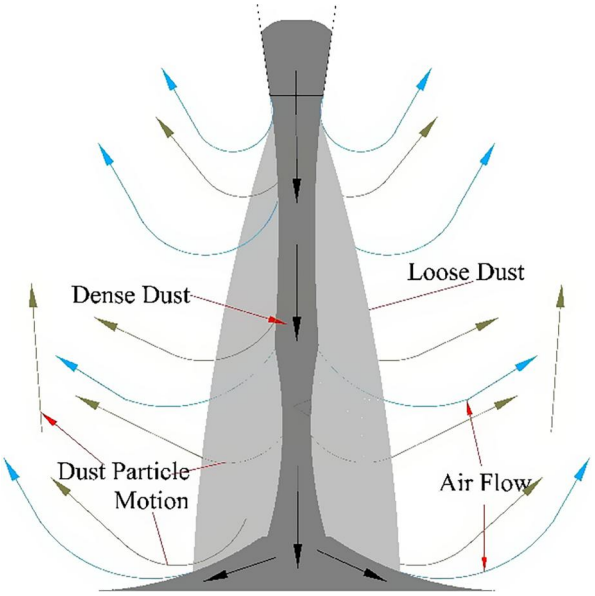

Figure 2. Dust generation processes in the free-falling powder: dust generation from the falling powder stream (upper part of figure); dust generation from the splash from the powder-covered surface (lower part of figure).

stream impacting the bottom surface, generate strong vorticity in the vicinity of the bottom surface, which suspends previously deposited particles.

Our simulations study the aerodynamic dust generation resulting from the impact of the falling powder with the bottom surface. Falling agglomerates, or the collective motion of the falling powder, are modeled as a falling pellet disk. The pellet remains intact in this simulation. The powder hill at the base of the powder stream is modeled as a layer of particles. In our simulations, this layer of particles is released slightly above the bottom surface within 0.1 s after the powder pellet impact. A result of our simulations is that the backflow generated by the falling disk (vortex shedding) is much more efficient than that from an impinging piston whose backflow at the surface merely derives from the displaced air ahead of the piston. A schematic of these simplifications is shown in the online supplemental information (SI, Section S-1).

The model geometry is inspired by the Heitbrink experiments (Heitbrink, Baron, and Willeke 1992). The test chamber is a column of 75 cm in height with a square 12×12 cm base. The standard pellet in the simulations is a cylindrical disk of 4 mm radius and 3 mm thickness. The size of the pellet is clearly much larger than a typical agglomerate; however, we argue (see the SI—Section S-6) that the physics of the splash process is relatively insensitive to the size of the pellet. For specificity, the powder and pellet are modeled as silica, with density $\rho = 2000\,\mathrm{kg/m^3}$; the pellet has a mass of 3.0144×10^{-4} kg. It is released from the top of the test chamber; for numerical stability of the simulation, the release is gradually ramped up, with the full gravitational acceleration only achieved after $\Delta t = 0.25$ s. Physically, the orientation of a falling disk would be unstable, with the disk tumbling (Field et al. 1997; Zhong, Chen, and Lee 2011; Zhong et al. 2013); in our simulations, the disk is constrained to fall with its flat always oriented horizontally, i.e., parallel to the bottom surface. Again, for numerical stability of the simulation, the pellet disk is not allowed to impact the bottom of the test chamber, but rather, the fall of the disk is halted 1 mm above the bottom of the test chamber. Halting the pellet descent just before impact also isolates the aerodynamic resuspension mechanism (studied here) from other forces between the pellet and the particles that are to be resuspended.

The final velocity of the pellet is 3.64 m/s, achieved at $\Delta t \sim 0.515$ s from release. The final velocity is reduced by 10% due to the ramping up of gravity; similarly, the impact time is delayed by 32% due to the ramping up of gravity. Only the final impact velocity is relevant for the dust cloud generation. This final velocity is only $1/4$ of the estimated terminal velocity (balancing gravitational acceleration against Stokes drag). For a discussion of the terminal velocity of disk-shaped particles, see Zhou et al. (2022). Since all velocities are low, the air is treated as incompressible. The Reynolds number for this final air flow around the pellet is Re $\sim$ 1860. For $40 < \mathrm{Re} < 105$, the flow pattern is expected to be symmetric about the central axis of the disk, with a recirculation zone behind the disk. For Re $\sim$ 105, the wake behind the disk is expected to lose axial symmetry, with long thin thread-like wakes extending behind a pair of recirculation zones (Natarajan and Acrivos 1993; Zhong and Lee 2012). Periodic vortex shedding is expected to occur for Re $>$ 118 (Bearman and Takamoto 1988; Fabre, Auguste, and Magnaudet 2008; Miau et al. 1997; Shenoy and Kleinstreuer 2008; Zhong and Lee 2012). Vortex generation behind accelerating and decelerating disks has also been studied (Sallet 1975; Steiner et al. 2023; Taylor 1953; Yang, Jia, and Yin 2012).

Spherical particles are uniformly distributed as a monolayer at the bottom of the chamber and are released at $\Delta t = 0.6$ s after the release of the disk at the top, i.e., within 0.1 s after the disk is stopped at the bottom. Releasing the particles just above the substrate deliberately neglects particle-substrate interactions (the focus of traditional resuspension studies, which emphasize overcoming the adhesion forces to

the substrate). There are no particle-particle interactions and no particle agglomeration or break-up. Particle collisions with the chamber wall are treated as elastic. The simulations are athermal. The simulations are thus designed to isolate and highlight the role of aerodynamics in the resuspension process.

2.2. Numerical methods

We have used STAR-CCM+ (2023) as the CFD simulation software in this study. STAR-CCM+ can easily track massive particle trajectories. For a general discussion of modeling dilute particle-laden flows, see Chen and Wood (1985), Crowe (1998), Curtis and van Wachem (2004), Schwarzkopf, Crowe, and Dutta (2009), Tsuji, Morikawa, and Shiomi (1984), and Zhang and Reese (2001).

2.3. Grid generation

The domain is the Heitbrink chamber ($75 \times 12 \times 12$ cm). Unstructured grids (Ferziger, Peric, and Street 2019) were generated within STAR-CCM+; the basic cell is a 3 mm cube ('trimmed cell') in the bulk of the domain and flattened rectangular prisms at the disk boundary surface. Near the bottom surface ($5 \times 12 \times 12$ cm), the grid is 50% refined (refined cell is a 1.5 cm cube). The central column ($75 \times 5 \times 5$ cm) is also 50% refined. The total cell count is 1,131,386. The falling disk is treated as a moving part. The refined grid in the central cylinder rigidly moves with the falling disk. A schematic of the grid geometry is given in the SI (Section SM-2).

2.4. Numerical simulation method

2.4.1. Air flow only

The final velocity of the pellet is $v_f = 3.64$ m/s. This sets the velocity scale of the air flow in the chamber, whence $v/c_{\text{sound}} < 10^{-2}$, where c_{sound} is the velocity of sound in air; the flow is thus incompressible. The final pellet velocity is achieved at $\Delta t \sim 0.54$ s from release; note that this is only ¼ of the terminal velocity (balancing gravitational acceleration against Stokes drag). The Reynolds number for this final air flow around the pellet is Re ~ 1860. The air flow near the bottom surface is smaller and quickly dissipates after pellet impact; the air flow is thus treated as laminar.

The finite volume method (FVM) is used to discretize the governing equations. The discretization of equations and domain, as well as the iterations of discretized equations, are all conducted using the commercial FVM solver within STAR-CCM+. The convection terms are discretized using a second-order Upwind Scheme. The transient terms are discretized by a second-order Temporal Scheme. The time step is set at $\Delta t = 0.0025$ s, and the simulation is run for $\Delta T = 40$ s. The discretized governing equations are solved using the SIMPLE (Semi-Implicit Method for Pressure Linked Equations) algorithm. Velocity and pressure under-relaxation factors are 0.9 and 0.5, respectively. The falling disk is incorporated using rigid motion of the core cylindrical grid. The solution of the equations was considered to be converged when the scaled residuals for the continuity and momentum equations decreased to 10^{-5} for each time step. Grid independence of the air flow solutions is discussed in the SI—Section S-3.

2.4.2. Addition of particles—Lagrangian multiphase approach

To simulate the dust cloud lofting, the particles are initially distributed uniformly on the bottom of the entire chamber. The number of particles in the simulations was $N = 10^4$ for the dustiness simulations and $N = 10^2$ for the particle track simulations. Particles are injected at $t = 0.6$ s (using the Star CCM+ Parcel Injector) with an initial upward velocity of $v = 1 \times 10^{-6}$ m/s.

Lagrangian Multiphase flow (Subramaniam 2013; Tartakovsky, Ferris, and Meakin 2009) incorporates air-particle interaction by adding air source terms into the Navier-Stokes equations (Andrews and O'Rourke 1996; Crowe 1998; Crowe, Troutt, and Chung 1996; Crowe et al. 2011; Patankar and Joseph 2001a, 2001b; Schwarzkopf, Crowe, and Dutta 2009; Snider, O'Rourke, and Andrews 1998). For a dilute dust cloud (volume fraction $\phi < 10^{-3}$), the main air-particle forces (Crowe et al. 2011) are drag (Schiller and Naumann 1935; Stokes 1851) and particle shear-lift (Saffman 1965); gravitational body force is incorporated in the usual way.

Tracking of massive particles is incorporated *via* the Lagrangian-Euler Method with two-way coupling between the air continuum and the dispersed particulate phase. Particle–particle interactions are neglected. Particle agglomeration and breakup are also neglected since aerodynamic shear forces are insufficient to break up agglomerates. For the Heitbrink geometry, we do not expect particle impact on the chamber walls, which, in principle, might induce breakup, so this also has been neglected. The infrequent interaction of the particles with the chamber walls has

been specified to be purely elastic (i.e., unit coefficient of restitution), so no particles stick to the chamber walls.

In the Lagrangian-Euler Method, the motion of each dust particle in the Lagrangian frame is given by:

$$m_p \frac{dv_p}{dt} = F_d + F_p + F_{LS} + m_p g \tag{1}$$

where m_p and v_p are the mass and velocity of the particle and g is the gravitational acceleration. The drag force, F_d, and pressure force, F_p, are given below. The drag force (in a direction opposite to the motion of the particle) is given by

$$F_d = \frac{1}{2} C_d \rho A_p v_r^2 \tag{2}$$

where $A_p = (\pi/2)\ D_p{}^2$ is the particle cross-sectional area, D_p is the particle diameter, ρ is the density of air, and the relative particle-air velocity $v_r = u - v_p$, where u is the local air velocity, v_p is the local particle velocity, and where C_d is the Schiller-Naumann particle drag coefficient (1935). The pressure gradient force is given by

$$F_p = -V_p \nabla p_{static} \tag{3}$$

where $V_p = (\pi/6)\ D_p{}^3$ is the particle volume, and ∇p_{static} is the gradient of the static air pressure. There is an additional Safman lift force, F_{LS}, on each particle, due to shear near the walls (Saffman 1965).

We have used two-way coupling for these simulations. A result of our simulations is that the particles remained well-dispersed in the cloud; the aerosol is thus sufficiently dilute so that one-way coupling would have been sufficient. However, we wanted to admit the possibility of particles accumulating in a localized region of the cloud, in which case, the feedback of the particle motion on the fluid would become important, necessitating two-way coupling.

In two-way coupling, the rate of momentum transfer from the particles back to the continuum air phase is achieved by augmenting the Navier-Stokes equations with a sink term

$$S_V = -\sum\nolimits_n F_d^n \delta t_n / \Delta t \tag{4}$$

where the sum is over all particles n in the given cell during the computed time step, $F_d{}^n$ is the drag force (2) exerted by the fluid on the nth particle, and $\delta t_n/\Delta t$ is the fraction of time that the nth particle spends in the given cell during this time step.

3. Results and discussion

3.1. Airflow of the standard falling pellet

We first discuss the air flow generated by the falling pellet disk ($R = 4$ mm, $t = 3$ mm). As the disk falls, it induces air motion within the chamber (SI Figure S-5). After $\Delta t \sim 0.3$ s, Re $>$ 100, and vortices are shed behind the disk; the flow behind the disk is asymmetric and unstable. Air ahead of the disk is quiescent. The disk "impacts" the bottom of the chamber at $t = 0.54$ s. Particles will be released at 0.6 s. As the pellet impacts, the edges of the disk are regions of high vorticity (SI Figure S-6). Radial and upward air flow has the potential to loft particles up from the surface and aerosolize a dust cloud.

Figure 3 shows the vertical velocity, v_y, on the central midplane ($z = 0$) just before ($t = 0.5$ s—panel a) and just after impact ($t = 0.6$ s—panel b); height axis is left-to-right (the top of the chamber is at left; the base of the chamber is at right); cross-plane distance is front-to-back. We are particularly interested in the air flow induced at the base of the chamber, which will be instrumental in lofting dust from the monolayer. Before impact, the downward vertical velocity is confined to the wake immediately *behind* the disk (there is negligible flow ahead of the disk, arguing against the importance of piston-like flow driving dust dispersion); a small region of upward velocity exists just outside the disk, presumably from the attached vortex ring around the disk. Upon impact, the region of upward velocity extends from the disk radius outwards all the way toward the chamber walls. A full time sequence of the evolution of the vertical velocity is given in the SI (Figure S-7).

Figure 4 shows the out-of-plane vorticity magnitude, $|\omega_z|$, on the central midplane ($z = 0$) just before ($t = 0.5$ s—panel a) and just after impact ($t = 0.6$ s—panel b); height axis is left-to-right (the top of the chamber is at left; the base of the chamber is at right); cross-plane distance is front-to-back. Again, we are interested in the air flow induced at the base of the chamber, which will be instrumental in lofting dust from the monolayer. Before impact, there is large positive/negative vorticity on the right/left of the disk, indicative of the vortex ring attached to the disk; again, vorticity is confined to the wake *behind* the pellet. Upon impact, the vorticity dissipates radially. We interpret this behavior as the detachment of the bound trailing vortex ring upon deceleration of the pellet. A full sequence of the out-of-plane vorticity, ω_z is given in the SI (Figure S-8).

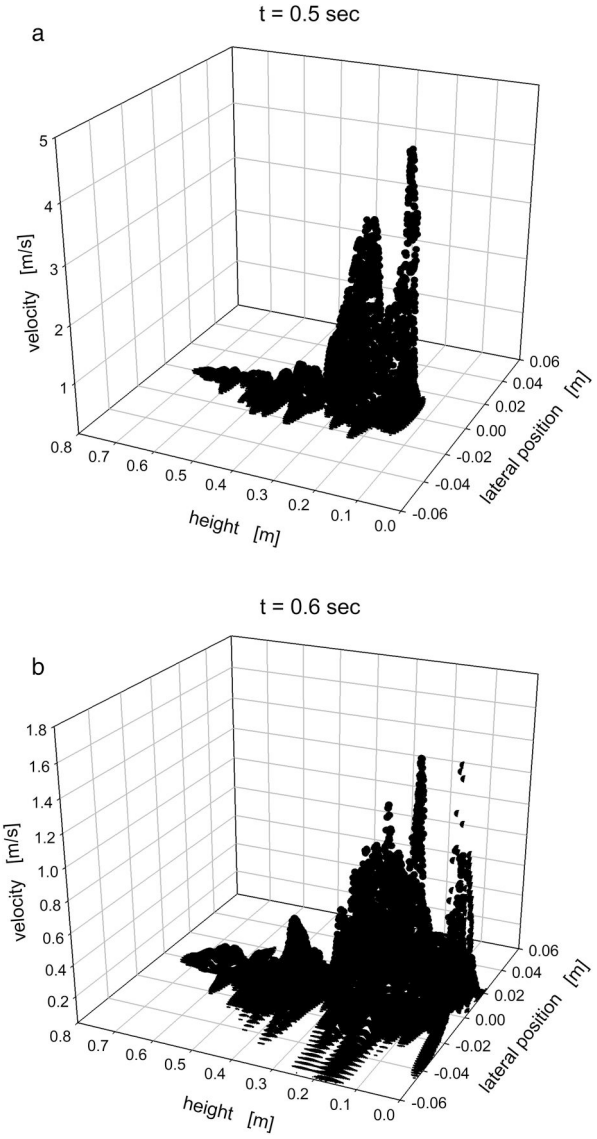

Figure 3. Vertical velocity, v_y, on the central midplane ($z = 0$): (a) $t = 0.5$ s, (b) $t = 0.6$ s.

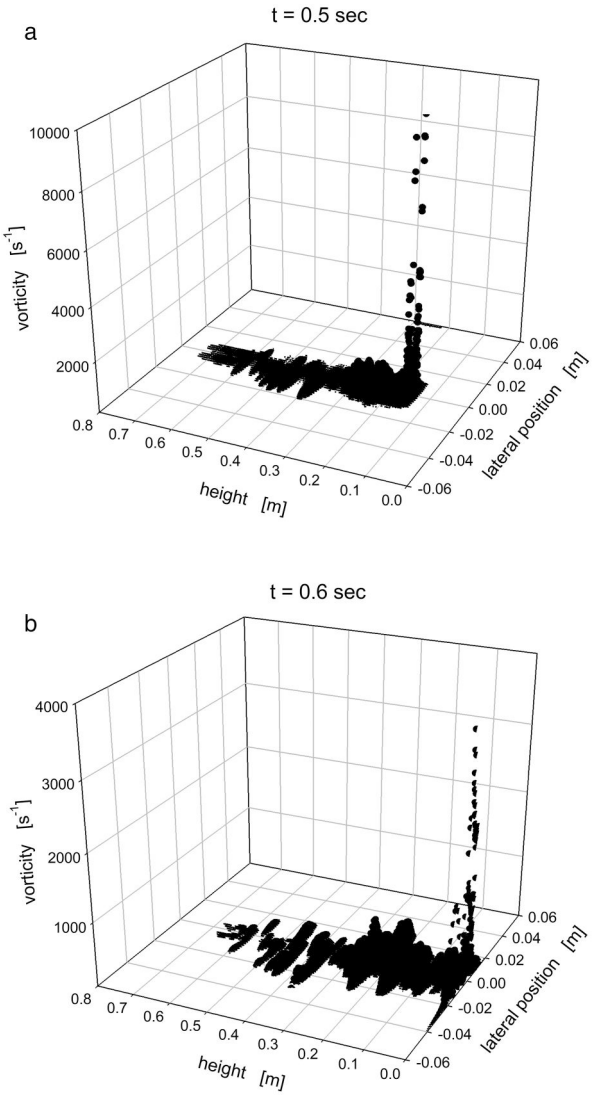

Figure 4. Out-of-plane vorticity magnitude, $|\omega_z|$, on the central midplane ($z = 0$): (a) $t = 0.5$ s, (b) $t = 0.6$ s.

3.2. Standard pellet—standard dust

In this section, we discuss the dust cloud generated by the impact of the standard pellet disk ($R = 4$ mm, $t = 3$ mm) on a monolayer of 1 μm silica particles. The dust cloud develops with time, as shown in Figure 5. The pellet has impacted at $t = 0.54$ s (before the first panel). The wake behind the decelerated disk evinces the residual motion (velocities depicted with the color scale) due to previous vortex shedding; this persists for long time (it is still apparent at $t = 20$ s). At the bottom of the chamber, the lofted particle dust cloud is indicated in dark blue. Due to the small particle size ($d = 1$ μm), the dust cloud does not settle with time. Note the scale: the chamber height is 75 cm; the apparent dust cloud height is of the order of several cm.

Pictures showing the temporal evolution of dustiness, average height, and radius of the dust cloud are given in the SI (Section S-5). For the purposes of the simulation, dustiness is operationally defined as the fraction of particles that are lofted above $y = 5$ mm. Figure S-9 displays the dustiness as a function of time. Within 0.5 s of impact, 14% of the monolayer has been aerosolized (note that the magnitude of this fraction is somewhat arbitrary, as it would be reduced for a chamber of larger base size). This time for aerosolization is comparable to what we observed (0.3 s) in our visualization of the splash process (Figure 1). Due to their small size, the particles remain suspended for the duration of the simulation (40 s). The persistence of the splash dust cloud is consistent with our observation (Figure 1).

Figure S-10 displays the height of the dust cloud. The maximum height (height of the highest particle)

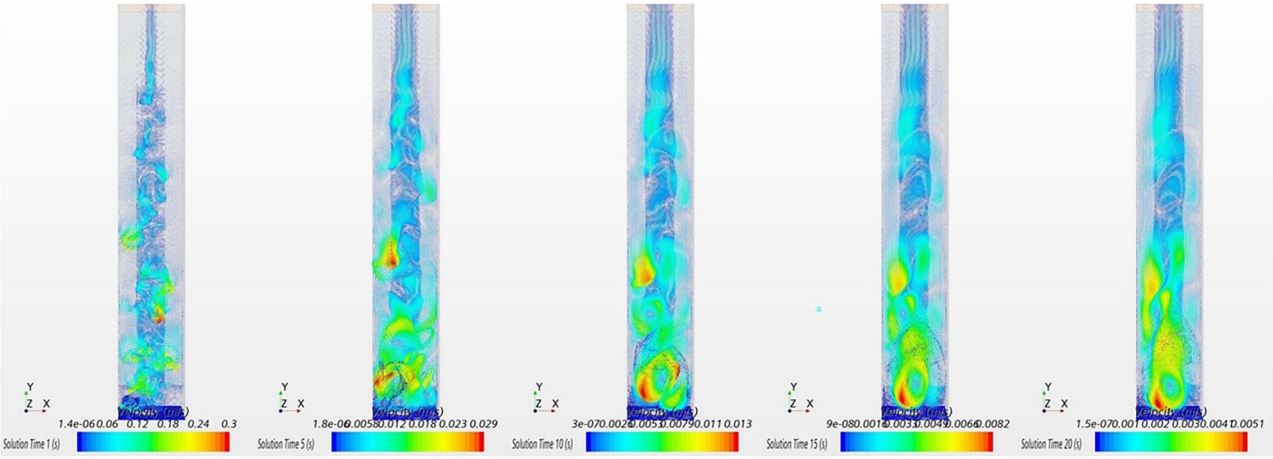

Figure 5. Dust cloud of 1 μm particles (from left to right, 1, 5, 10, 15, and 20 s).

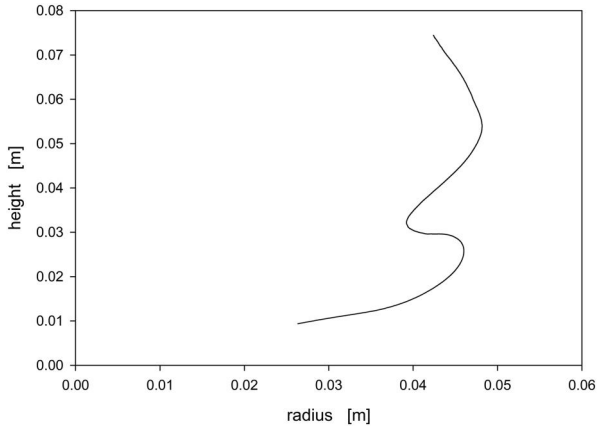

Figure 6. Trajectory of the dust cloud centroid for the standard pellet disk ($R = 4$ mm, $t = 3$ mm) falling on a monolayer of 1 μm silica powder—the dust cloud starts near the floor ($r = 0.026$ m, $h = 0.009$ m) at $t = 0.6$ s and is lofted ($r = 0.043$ m, $h = 0.073$ m) at $t = 10$ s.

is ~20 times the average height (averaging the height over all particles). This indicates that the dust cloud density decreases with height, as expected. It also indicates that the dust cloud is not vertically well-mixed over its entire height. The constancy of that ratio suggests that the structure of the dust cloud does not change with time. The lack of vertical mixing is consistent with our observation (Figure 1).

Figure S-11 displays the average radius of the dust cloud (averaging the radial location over all particles). Within 0.5 s, the extent of the dust cloud quickly expands to 4.5 cm, which is an order of magnitude larger than the disk radius, and seems to be limited by the confining walls of the chamber; we cannot measure the intrinsic radius (with no confining chamber walls) of the dust cloud in these simulations. The small undulation for $2\,\text{s} < t < 6\,\text{s}$ suggests that while the cloud is initially propelled outward, it undergoes a minor retraction during this time interval (possibly driven by the motion of the vortex ring detaching from the fallen disk). The simulation lateral extent (4.5 cm) is larger than that of our visualization (Figure 1), but our experimental dust cloud may be more confined due to the retaining wall of the Plexiglas tray into which the powder falls.

The average dust cloud height and radius may be combined to monitor the trajectory of the dust cloud centroid (note that this is not the center of mass, which would be located at $r = 0$, above the pellet). Figure 6 displays the trajectory of the centroid for $0.6\,\text{s} < t < 10\,\text{s}$. The dust cloud starts near the floor ($r = 2.6$ cm, $h = 9$ mm) at $t = 0.6$ s and is propelled outward and lofted ($r = 43$ cm, $h = 7.3$ cm) at $t = 10$ s. At intermediate times ($t \sim 2$ s), there is a slight retraction in radius with no additional lofting, and then lofting recommences with an additional expansion; at later times ($t > 8$ s) there is a slight retraction as lofting continues but is considerably slowed.

We have also conducted simulations where the initial monolayer of particles does not cover the entire floor of the chamber but rather is confined to a sequence of annuli around the pellet impact point. This allows a calculation of dustiness as a function of radial distance from the impacting disk (Figure 7). Note that this dustiness "profile" does not give information on the structure of the dust cloud; rather, it represents the probability of resuspension as a function of distance from the impacting disk. As expected, aerosolization is complete (dustiness ~ 1) near the impacting disk; the probability decreases to ~0.5 at ~5 times the radius of the disk; the probability effectively vanishes at ~10 times the radius of the disk. This dustiness profile is time-independent, reflecting the lack of settling of the dust cloud of 1 μm particles.

We also can follow the centroid trajectory of the cloud resuspended from each of these annular monolayers (Figure S-12). Each annulus, once resuspended, is propelled radially outward as lofting progresses.

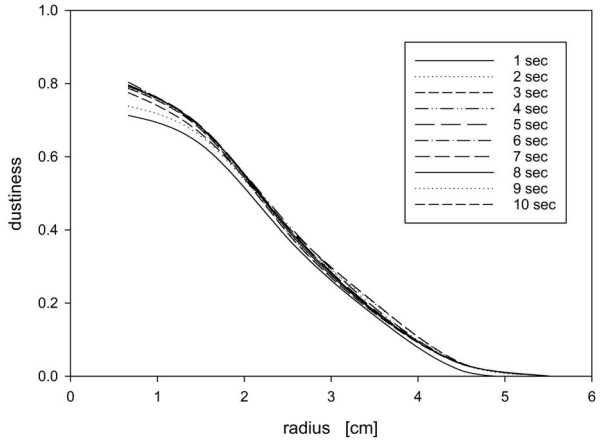

Figure 7. Dustiness profile—probability of aerosolization as a function of radial distance from the impacting pellet disk.

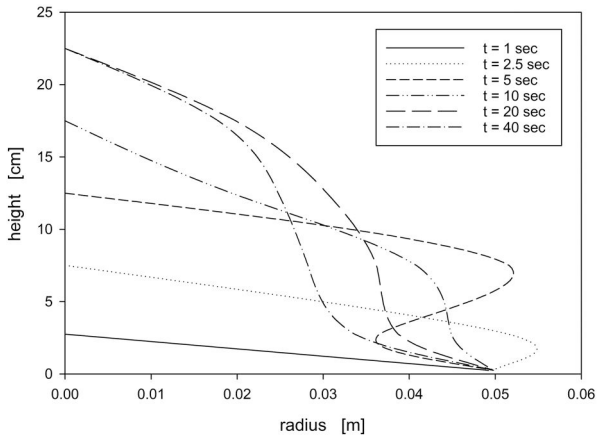

Figure 8. Average radius within each height slab, inverted to provide a profile of the dust cloud: $t = 1$, 2.5, 5, 10, 20, 40 s.

Each annulus experiences a retraction ($2\,\text{s} < t < 4\,\text{s}$) before it resumes expansion and lofting. For $t > 4$ s, the trajectories of all but the outermost annulus coincide, suggesting radial mixing of the particles originating from these different annuli.

We have also monitored the number of particles aerosolized to different height slabs (0–0.5, 0.5–5, 5–10, 10–15, 15–20, 20–25 cm). Inverting the measured average particle radius within each height slab permits a determination of the dust cloud profile (Figure 8). For small times ($t = 1$ s), the dust profile monotonically decreases away from the fallen pellet. At $t = 2.5$ s, the extrema of the cloud are propelled outward; at $t = 5$ s, intermediate heights are retracted inward. For $t > 10$ s, the dust profile returns to being monotonic, as the lofting proceeds. For $20\,\text{s} < t < 40\,\text{s}$, lofting has stabilized with the cloud retracting inward somewhat.

The model is relatively insensitive to variations in pellet radius and thickness (SI—Section S-6).

3.3. Dust particle size effects

We now study changes in the dust cloud as the size of the particle in the monolayer is changed. Dustiness (the fraction of particles that have been lofted above 5 mm height in the chamber) depends upon particle diameter (Figure 9). While the initial lofting of the dust cloud is independent of powder particle size, at longer times, gravitational settling reduces the particle population in the dust cloud. Gravitational settling is apparent at $d = 5$ μm; for $d = 7.5$ μm, the dust cloud settles over the timescale of the experiment ($t = 40$ s).

The depletion of particles from the dust cloud also affects the height of the dust cloud. We monitor this change by looking at the cloud centroid trajectories for powders of different particle diameters (Figure 10). For

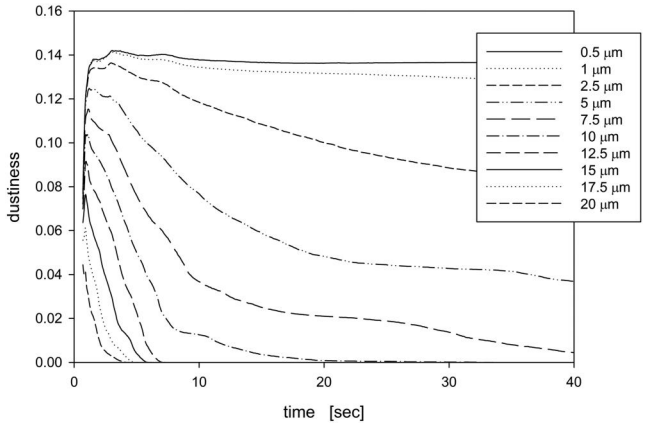

Figure 9. Dustiness (t) for dust cloud lofted by the standard pellet disk ($R = 4$ mm, $t = 3$ mm) for silica powder of various diameters (particle diameter in microns shown in legend at right).

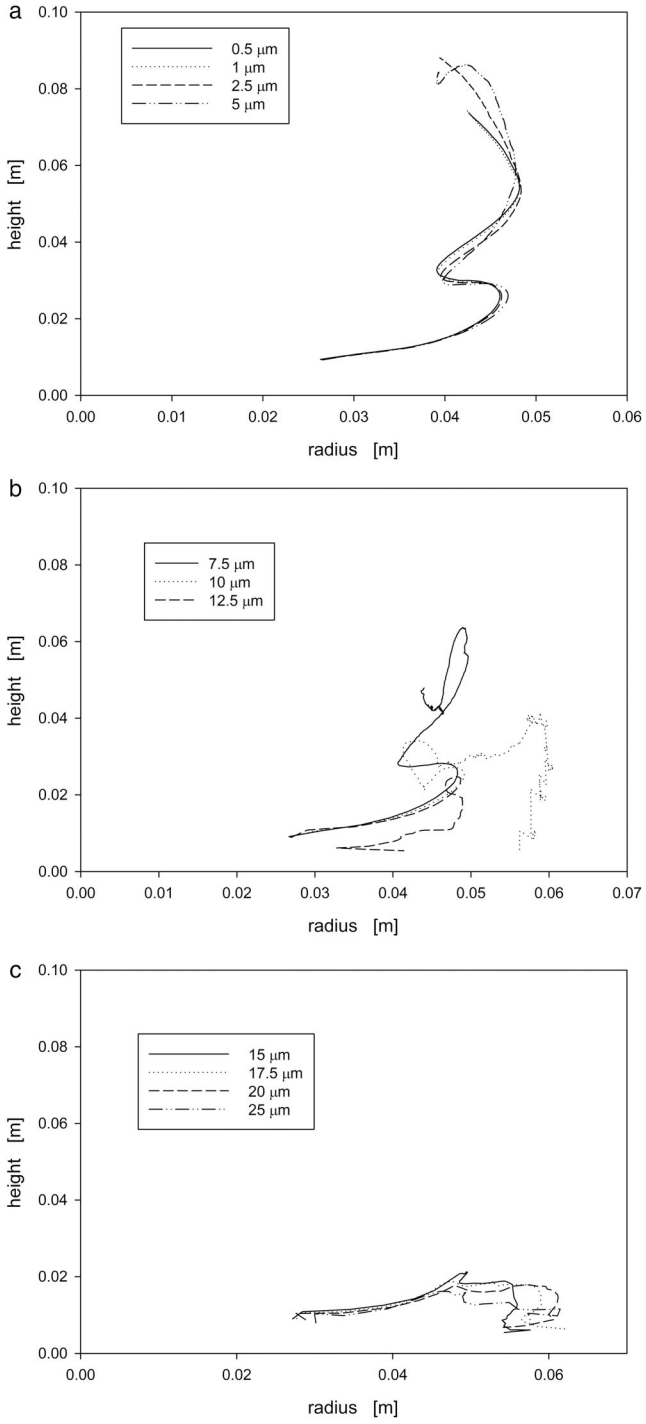

Figure 10. Dust cloud centroid trajectory for dust clouds of different particle sizes: (a) $d = 0.5$, 1, 2.5, 5 μm; (b) $d = 7.5$, 10, 12.5 μm; (c) $d = 15$, 17.5, 20, 25 μm.

particles with $d < 5$ μm, the trajectories are identical to those of the 1 μm dust cloud; for particles with $d > 15$ μm, gravitational settling precludes significant lofting; dust clouds for the intermediate particle sizes exhibit erratic cross-over between the small and large particle clouds.

Taking vertical sections, we may track the change in the temporal dust cloud profile as a function of particle size (Figure 11). Cloud height begins to decrease at $d = 5$ μm and is significant at $d = 10$ μm. The radial cloud retraction ($t \sim 5$ s) is apparent for clouds with $d < 7.5$ μm.

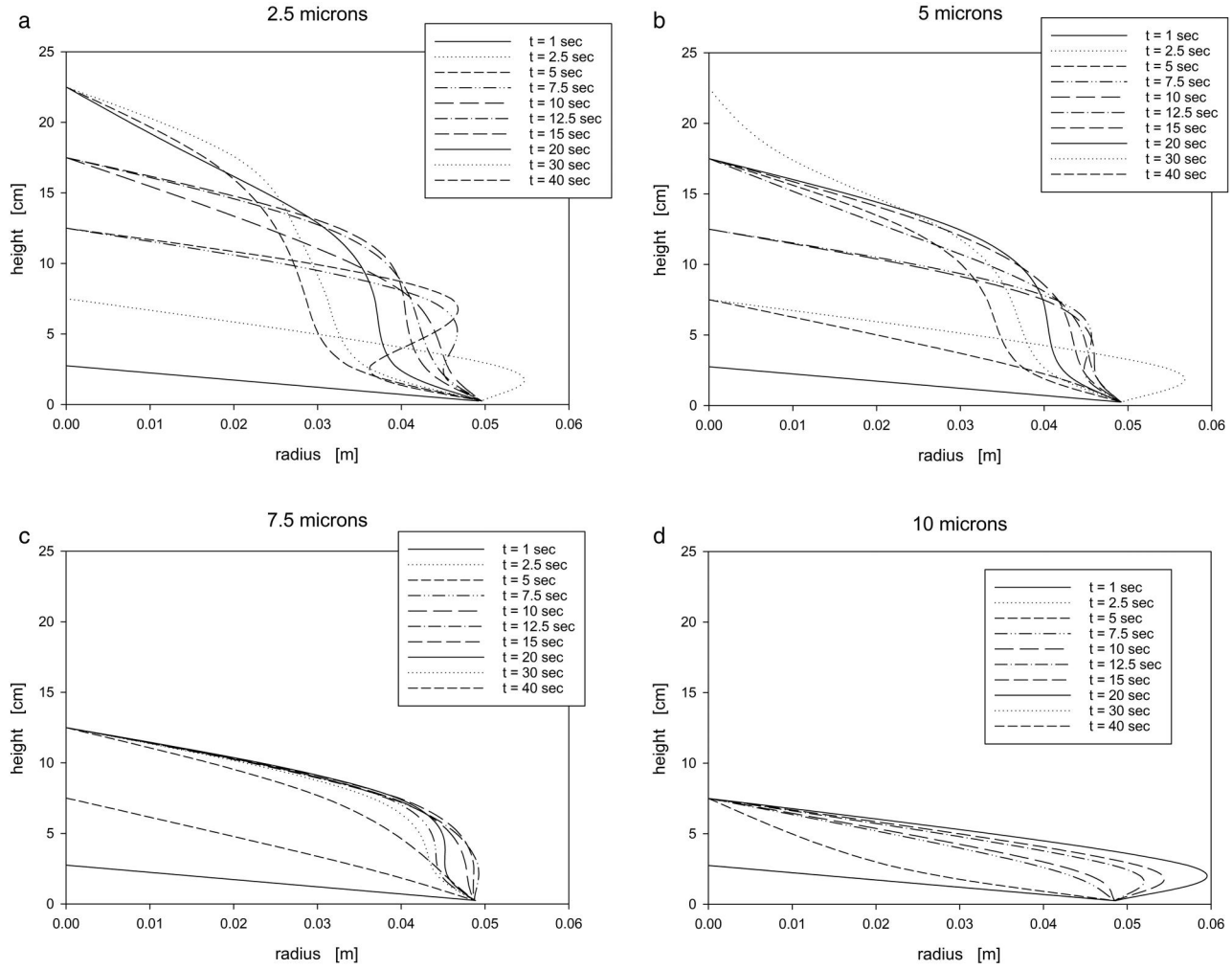

Figure 11. Dust cloud profile for various times (listed in legend at right) for clouds of particles of different particle sizes: (a) $d = 2.5\,\mu m$; (b) $d = 5\,\mu m$; (c) $d = 7.5\,\mu m$; (d) $d = 10\,\mu m$.

4. Discussion–relevant aerodynamics

Eames and Dalziel (2000) studied experimentally the hydrodynamic resuspension of dust particles from a surface due to the flow disturbance generated by an impacting body ($300 < \mathrm{Re} < 3500$). They concluded that dust resuspension occurs if the Shields criterion (1936) (developed for horizontal transport of sediment by a turbulent parallel flow) is satisfied. The particle Shields parameter is defined as

$$\theta_P = \left[\rho_f/(\rho_P - \rho_f)\right] U^2/gd \qquad (5)$$

where U is the impacting velocity and d is the particle diameter; ρ_p and ρ_f are, respectively, the particle and fluid densities. Resuspension occurs when $\theta_p > \theta_c$ where the critical Shields parameter $\theta_c \sim 5/\mathrm{Re}_p^{1/2}$ for $\mathrm{Re}_p < 1$ and $\theta_c \sim 3$ for $\mathrm{Re}_p > 1$, where Re_p is the particle Reynolds number. Figure 12 displays the maximum diameter of a Shields suspendable dust particle at a given impact velocity, U; our simulations (vertical line at $U = 3.64$ m/s) are all consistent with the Shields criterion.

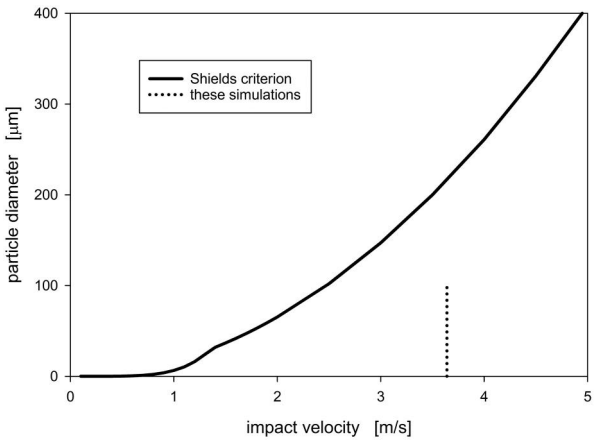

Figure 12. Maximum diameter of suspended sediment particle (as determined by the Shields criterion) as a function of the impact velocity of the falling pellet. The vertical line (at $v = 3.64$ m/s) indicates the simulations of this study.

Sutherland (1967) imaged the motion of a grain on a surface, due to an impacting vortex ring (generated by a pulsating normal jet); he reported a threshold pulse frequency for the generation of particle motion and crater formation in the sediment. Wells (1992) and Wells and Hopfinger (1993) studied trajectories and kinematics of individual particles suspended by the impact of a low Re $\sim$ 25 vortex ring; the Wells trajectories closely resemble the dust centroid trajectories of our study (Figures 6, 10, S-12). Munro, Bethke, and Dalziel (2009) studied the crater formation in a sediment due to the normal impact of a vortex ring (Re $\sim$ 5000).

The interaction of a vortex ring directly impacting a wall has been extensively studied (Chu, Wang, and Chang 1995; Gendrich, Bohl, and Koochesfahani 1997; Mishra, Pumir, and Ostilla-Mónico 2021; Naguib and Koochesfahani 2004; Orlandi and Verzicco 1993; Ren, Zhang, and Guan 2016; Ren and Lu 2015; Swearingen, Crouch, and Handler 1995; Walker et al. 1987; Xu et al. 2017; Xu and Wang 2013). However, our current simulations suggest that the lofting aerodynamics derives from a vortex ring *shed* by the decelerating disk rather than the direct impacting of the vortex ring on the wall.

A real powder consists of primary particles, aggregates, and agglomerates, held together by forces of different strengths (aggregates being more strongly bound than the larger agglomerates). None of this complexity is included in our model; in particular, we have neglected break-up processes of the agglomerates, clearly important as the agglomerate impacts the surface. We have focused on the aerodynamic source (a falling agglomerate) resuspending the smaller particles (primary particles or smaller aggregates) previously deposited on the surface. In addition, we have neglected any particle-surface interactions, which must be overcome to effect the resuspension.

The actual dust cloud generated from the splash of a real falling powder will result from contributions from a population of falling aggregates, with a distribution of sizes and arrival times. Modeling the time evolution of real dust clouds will necessitate incorporating the statistics of this impacting population of aggregates, convoluted with a distribution of arrival times.

5. Conclusion

We have studied dust generation from the splash of a falling powder on a solid surface. This has been modeled as the aerodynamic resuspension of particles from the bottom surface due to the aerodynamic back flow induced by a pellet disk impacting the bottom surface.

In the model, a layer of primary particles is loosely distributed at the bottom of the chamber. A pellet disk (which models a larger aggregate) is released and falls freely to the bottom surface under gravity. Backflow is generated by the vorticity shed from the decelerating disk; particles are suspended by this shed vorticity. We have studied the structure (dustiness profile, dust cloud profile) and dynamics (centroid trajectory) of the dust cloud. We have examined changes in the dust cloud with the size of the suspended primary particles. The model is relatively insensitive (resulting in only minor changes in the dust cloud) to changes in the structure (radius and thickness) of the falling pellet disk.

We believe that this aerodynamic resuspension mechanism is important for dust generation in a variety of industrial processes (powder pouring, spilling, and conveyor transferring). The model provides an initial attempt to calculate the structure and evolution of the dust cloud produced by such processes.

While the isolated splash process has not been utilized as a stand-alone dustiness measurement technique, a qualitative observation may be made. Given its intermediate aerodynamic strength (Re $\sim 10^3$), the splash of falling powders is anticipated to generate more dust than the gentler rotating drum (Re $\sim 10^2$) but less dust than the aggressive Venturi (Re $\sim 10^4$) techniques. The present study does not yield information as to the partitioning of falling powder dust generation between the intrinsic and splash processes.

Disclaimer

The findings and conclusions of this article are those of the authors and do not necessarily represent the views of the National Institute for Occupational Safety and Health, Centers for Disease Control and Prevention. Mention of any product or company name does not constitute endorsement by the National Institute for Occupational Safety and Health, Centers for Disease Control and Prevention.

Acknowledgments

We thank D. E. Evans (NIOSH) for a careful reading of the manuscript. We thank J. Bennett, K. H. Dunn, D. E. Evans (all of NIOSH), and U. Ghia (U. Cincinnati) for helpful discussions. We thank B. Alexander, D. R. and D. R. Farwick (all of NIOSH) for help with the dust cloud visualization. We thank J. C. Wells (Ritsumeikan U., Kyoto, Japan) for

sharing a copy of his thesis, which documents the trajectories of individual particles lofted by Re = 25 vortex rings.

Disclosure statement

No potential conflict of interest was reported by the author(s).

Funding

This work was supported by the NIOSH Nanotechnology Research Center (NTRC project 939-0G00).

ORCID

Leonid A. Turkevich http://orcid.org/0000-0002-2831-2140

References

Andreasen, A. H. M., N. Hofman-Bang, and N. H. Rasmussen. 1939. Über das Staübungsvermögen der Stoffe [On the ability of materials to be dusty]. *Kolloid-Zeitschrift und Zeitschrift für Polymere* 86 (1):70–7. doi: 10.1007/BF01512003.

Andrews, M. J., and P. J. O'Rourke. 1996. The multiphase particle-in-cell (MP-PIC) method for dense particulate flows. *Int. J. Multiphase Flow* 22 (2):379–402. doi: 10.1016/0301-9322(95)00072-0.

Ansart, R., A. de Ryck, and J. A. Dodds. 2009. Dust emission in powder handling: Free falling particle plume characterization. *Chem. Eng. J.* 152 (2–3):415–20. doi: 10.1016/j.cej.2009.04.070.

Ansart, R., A. de Ryck, J. A. Dodds, M. Roudet, D. Fabre, and F. Charru. 2009. Dust emission by powder handling: Comparison between numerical analysis and experimental results. *Powder Technol.* 190 (1–2):274–81. doi: 10.1016/j.powtec.2008.04.053.

Ansart, R., J.-J. Letourneau, A. de Ryck, and J. A. Dodds. 2011. Dust emission by powder handling: Influence of the hopper outlet on the dust plume. *Powder Technol.* 212 (3):418–24. doi: 10.1016/j.powtec.2011.06.022.

ASTM. 1980. *Standard test method for index of dustiness of coal and coke*. ASTM standards 26: ANSI/ASTM D-547-41.

ASTM. 2021. *D6393/D6393M standard test method for bulk solids characterization by Carr indices – Measurement of Carr dispersibility (using the Hosokawa Micron International PT-X powder characteristics tester)*. West Conshohocken, PA: ASTM International (ASTM).

Baker, K. D., R. L. Stroshine, K. J. Magee, G. H. Foster, and R. B. Jacko. 1986. Grain damage and dust generation in a pressure pneumatic conveying system. *Trans. ASAE* 29 (3):0840–7.

Bearman, P. W., and M. Takamoto. 1988. Vortex shedding behind rings and disks. *Fluid Dyn. Res.* 3 (1–4):214–8. doi: 10.1016/0169-5983(88)90068-8.

Berger-Schuun, A., Geisenberger, J., Krayer, M., Leaver, A. T., Oeschm, H. P., Russell, D. B, and Uhrig, H. 1989. Bestimmung des Staubverhaltens von Farbstoffen [Determination of the dust behavior of dyes]. *Melliand Text. Rep.* 9:690–2.

BOHS. 1985. Technical Guide No. 4, Dustiness estimation methods for dry materials. In *Part 1: Their uses and standardization. Part 2: Towards a standard method. British Occupational Hygiene Society (BOHS). Technology Committee. Working Group on Dustiness Estimation*, ed. C. M. Hammond, N. R. Heriot, R. W. Higman, A. M. Spivey, J. H. Vincent, and A. B. Wells. Northwood: Science Reviews Ltd.

BOHS. 1988. Technology Committee: Working Party on dustiness estimation. British Occupational Hygiene Society (BOHS). *Ann. Occup. Hyg.* 32 (4):535–44.

Brouwer, D. H., I. H. M. Links, S. A. F. de Vreede, and Y. Christopher. 2006. Size selective dustiness and exposure; simulated workplace comparisons. *Ann. Occup. Hyg.* 50 (5):445–52. doi: 10.1093/annhyg/mel015.

Burdett, G. J., K. Y. Chung, D. Mark, L. A. Armbruster, and N. O. Breum. 2000. Development of a method for dustiness testing, EU contract SMT4-CT96-2074, HSE Report IR/L/MF/00/11, Health and Safety Laboratory, Sheffield.

Cawley, B., and D. Leith. 1993. Bench-top apparatus to examine factors that affect dust generation. *Appl. Occup. Environ. Hyg.* 8 (7):624–31. doi: 10.1080/1047322X.1993.10388170.

CEN. 1993. *EN 481 workplace atmospheres – Size fraction definitions for measurement of airborne particles*. Brussels: Comité de Européen Normalisation (CEN).

CEN. 2013. *EN 15051-3 workplace exposure – Measurement of the dustiness of bulk materials. Part 3: Continuous drop method*. Brussels: Comité de Européen Normalisation (CEN).

CEN. 2019. *EN 17199-3 workplace exposure – Measurement of dustiness of bulk materials that contain or release respirable NOAA and other respirable particles. Part 3: Continuous drop method*. Brussels: Comité de Européen Normalisation (CEN).

Chen, C., and P. Wood. 1985. A turbulence closure model for dilute gas-particle flows. *Can. J. Chem. Eng.* 63 (3): 349–60. doi: 10.1002/cjce.5450630301.

Chen, H., L. A. Turkevich, M. A. Jog, and U. Ghia. 2023. Numerical investigation of powder aerosolization in a mining rock dust dispersion chamber. *J. Loss Prev. Process Ind.* 83:105050. doi: 10.1016/j.jlp.2023.105050.

Chen, H., M. A. Jog, and L. A. Turkevich. 2023. Computational fluid dynamics simulations of aerosol behavior in a high-speed (Heubach) rotating drum dustiness tester. *Particuology* 72:68–80. doi: 10.1016/j.partic.2022.02.010.

Chen, H., M. A. Jog, D. E. Evans, and L. A. Turkevich. 2021. Numerical investigation of powder aerosolization in a rotating drum apparatus. *Powder Technol.* 390:62–72. doi: 10.1016/j.powtec.2021.04.102.

Chen, X., C. Wheeler, T. Donohue, R. McLean, and A. Roberts. 2012. Evaluation of dust emissions from conveyor transfer chutes using experimental and CFD simulation. *Int. J. Miner. Process.* 110–111:101–8. doi: 10.1016/j.minpro.2012.04.008.

Cheng, L. 1973. Formation of airborne respirable dust at belt conveyor transfer points. *Am. Ind. Hyg. Assoc. J.* 34 (12):540–6. doi: 10.1080/0002889738506895.

Chu, C.-C., C.-T. Wang, and C.-C. Chang. 1995. A vortex ring impinging on a solid plane surface—Vortex structure and surface force. *Phys. Fluids* 7 (6):1391–401. doi: 10.1063/1.868527.

Cleaver, J., and B. Yates. 1973. Mechanism of detachment of colloidal particles from a flat substrate in turbulent flow. *J. Colloid Interface Sci.* 44 (3):464–74. doi: 10.1016/0021-9797(73)90323-8.

Cowherd, C. Jr., M. A. Grelinger, and K. F. Wong. 1989. Dust inhalation exposures from the handling of small volumes of powders. *Am. Ind. Hyg. Assoc. J.* 50 (3):131–8. doi: 10.1080/15298668991374417.

Cowherd, C. Jr., M. A. Grelinger, P. J. Englehart, R. F. Kent, and K. F. Wong. 1989. An apparatus and methodology for predicting the dustiness of materials. *Am. Ind. Hyg. Assoc. J.* 50 (3):123–30. doi: 10.1080/15298668991374408.

Crowe, C. 1998. Turbulence modulation of fluid-particle flows—A basic approach. Third International Conference on Multiphase Flows.

Crowe, C. T., J. D. Schwarzkopf, M. Sommerfeld, and Y. Tsuji. 2011. *Multiphase flow with droplets and particles*. Boca Raton, FL: CRC Press.

Crowe, C. T., T. R. Troutt, and J. N. Chung. 1996. Numerical models for two-phase turbulent flows. *Annu. Rev. Fluid Mech.* 28 (1):11–43. doi: 10.1146/annurev.fl.28.010196.000303.

Curtis, J. S., and B. van Wachem. 2004. Modeling particle--laden flows: A research method. *AIChE J.* 50 (11):2638–45.

Dahmann, D., G. D. Hartfiel, and K. Mocklinghoff. 1997. Method for the realistic determination of the dustiness of bulk materials. *Gefahrst. Reinhalt. Luft* 57:503–9.

DIN. 1999. *Determination of a parameter for the dust formation of pigments and extenders—Part 2: Drop method*. DIN 55992-2, 6.

Donaldson, K., and A. Seaton. 2012. A short history of the toxicology of inhaled particles. *Part. Fibre Toxicol.* 9 (1):13. doi: 10.1186/1743-8977-9-13.

Dubey, P., U. Ghia, and L. A. Turkevich. 2017. Computational fluid dynamics analysis of the venturi dustiness tester. *Powder Technol.* 312:310–20. doi: 10.1016/j.powtec.2017.02.030.

Duffin, R., C. L. Tran, A. Clouter, D. M. Brown, W. MacNee, V. Stone, and K. Donaldson. 2002. The importance of surface area and specific reactivity in the acute pulmonary inflammatory response to particles. *Ann. Occup. Hyg.* 46:242–5.

Duffin, R., L. Tran, D. Brown, V. Stone, and K. Donaldson. 2007. Proinflammogenic effects of low toxicity and metal nanoparticles *in vivo* and *in vitro*: Highlighting the role of particle surface area and surface reactivity. *Inhal Toxicol.* 19 (10):849–56. doi: 10.1080/08958370701479323.

Eames, I., and S. B. Dalziel. 2000. Dust resuspension by the flow around an impacting sphere. *J. Fluid Mech.* 403:305–28. doi: 10.1017/S0022112099007120.

Evans, D. E. 2024. Quantification of airborne dusts from powders. In *NIOSH manual of analytical methods*. 5th ed., chapter AD. U.S. Department of Health and Human Services/Centers for Disease Control and Prevention/National Institute for Occupational Safety and Health (online). www.cdc.gov/niosh/nmam/pdf/Chapter_AD.pdf.

Evans, D. E., B. K. Ku, M. E. Birch, and K. H. Dunn. 2010. Aerosol monitoring during carbon nanofiber production: Mobile direct-reading sampling. *Ann. Occup. Hyg.* 54 (5):514–81.

Fabre, D., F. Auguste, and J. Magnaudet. 2008. Bifurcations and symmetry breakings in the wake of a disk. *Phys. Fluids* 20:051702.

Ferro, A. R. 2022. Resuspension. In *Handbook of indoor air quality*, ed. Y. Zhang, P. K. Hopke, and C. Mandin, chapter 12, 331. Singapore: Springer Nature.

Ferziger, J. H., M. Peric, and R. L. Street. 2019. *Computational methods for fluid dynamics*. 4th ed. Cham, Switzerland: Springer.

Field, S. B., M. Klaus, M. G. Moore, and F. Nori. 1997. Chaotic dynamics of falling disks. *Nature* 388 (6639):252–4. doi: 10.1038/40817.

Gendrich, C., D. Bohl, and M. Koochesfahani. 1997. Whole-field measurements of unsteady separation in a vortex ring/wall interaction. AIAA 28th Fluid Dynamics Conference, 1780. doi: 10.2514/6.1997-1780.

Hamelmann, F., and E. Schmidt. 2003. Methods of estimating the dustiness of industrial powders—A review. *KONA* 21:7–18. doi: 10.14356/kona.2003006.

Hamelmann, F., and E. Schmidt. 2004. Methods for characterizing the dustiness estimation of powders. *Chem. Eng. Technol.* 27 (8):844–7. doi: 10.1002/ceat.200403210.

Hamelmann, F., and E. Schmidt. 2005. Methods for dustiness estimation of industrial powders. *China Particuol.* 3 (1–2):90–3. doi: 10.1016/S1672-2515(07)60173-0.

Hammond, C. M. 1980. Dust control concepts in chemical handling and weighing. *Ann. Occup. Hyg.* 23 (1):95–109. doi: 10.1093/annhyg/23.1.95.

Heitbrink, W. A. 1990. *Aerosol generation by free falling powders and phantom particle creation by time-of-flight aerosol spectrometers*. PhD thesis, University of Cincinnati.

Heitbrink, W. A., P. A. Baron, and K. Willeke. 1992. An investigation of dust generation by free falling powders. *Am. Ind. Hyg. Assoc. J.* 53 (10):617–24. doi: 10.1080/15298669291360256.

Heitbrink, W. A., W. F. Todd, and T. J. Fischbach. 1989. Correlation of tests for material dustiness with worker exposure from the bagging of powders. *Appl. Ind. Hyg.* 4 (1):12–6. doi: 10.1080/08828032.1989.10389884.

Heitbrink, W. A., W. F. Todd, T. C. Cooper, and D. M. O'Brien. 1990. The application of dustiness tests to the prediction of worker dust exposure. *Am. Ind. Hyg. Assoc. J.* 51 (4):217–23. doi: 10.1080/15298669091369565.

Ibaseta, N., and B. Biscans. 2007. Ultrafine aerosol emissions from the free fall of TiO_2 and SiO_2 nanoparticles. *KONA* 25:190–204. doi: 10.14356/kona.2007017.

ISO. 1995. *7708. Air quality – Particle size fraction definitions for health-related sampling (reviewed and reconfirmed in 2017)*. Geneva: International Standards Organization (ISO).

John, W. 1995. Particle-surface interactions: Charge transfer, energy loss, resuspension, and deagglomeration. *Aerosol Sci. Technol.* 23 (1):2–24. doi: 10.1080/02786829508965291.

Kuhlbusch, T. A. J., C. Asbach, H. J. Fissan, D. Göhler, and M. Stintz. 2011. Nanoparticle exposure at nanotechnology

workplaces: A review. *Part. Fibre Toxicol.* 8 (1):22. doi: 10.1186/1743-8977-8-22.

Liden, G. 2006. Dustiness testing of materials handled at workplaces. *Ann. Occup. Hyg.* 50:437–9.

Lundgren, D. A. 1986. A measurement technique to quantitate fugitive dust emissions from handling granular products. *J. Aerosol Sci.* 17 (3):632–4. doi: 10.1016/0021-8502(86)90176-X.

Lundgren, D. A., and C. N. Rangaraj. 1986. A method for the estimation of fugitive dust emission potentials. *Powder Technol.* 47 (1):61–9. doi: 10.1016/0032-5910(86)80009-2.

Lyons, C. P., and D. Mark. 1992. An evaluation of the roaches 'dust particle apparatus' dustiness testing equipment. Contract Research Report No. 40/1992. Health and Safety Executive, UK. Her Majesty's Stationary Office (HMSO), London.

Miau, J. J., T. S. Leu, T. W. Liu, and J. H. Chou. 1997. On vortex shedding behind a circular disk. *Exp. Fluids* 23 (3):225–33. doi: 10.1007/s003480050106.

Mishra, A., A. Pumir, and R. Ostilla-Mónico. 2021. Instability and disintegration of vortex rings during head-on collision and wall interactions. *Phys. Rev. Fluids* 6 (10):104702. doi: 10.1103/PhysRevFluids.6.104702.

Munro, R. J., N. Bethke, and S. G. Dalziel. 2009. Sediment resuspension and erosion by vortex rings. *Phys. Fluids* 21: 046601.

Naguib, A. M., and M. M. Koochesfahani. 2004. On wall-pressure sources associated with the unsteady separation in a vortex ring/wall interaction. *Phys. Fluids* 16 (7): 2613–22. doi: 10.1063/1.1756914.

Natarajan, R., and A. Acrivos. 1993. The instability of the steady flow past spheres and disks. *J. Fluid Mech.* 254: 323–44. doi: 10.1017/S0022112093002150.

O'Shaughnessy, P. T., M. Kang, and D. Ellickson. 2012. A novel device for measuring respirable dustiness using low mass powder samples. *J. Occup. Environ. Hyg.* 9 (3):129–39. doi: 10.1080/15459624.2011.652061.

Orlandi, P., and R. Verzicco. 1993. Vortex rings impinging on walls: Axisymmetric and three-dimensional simulations. *J. Fluid Mech.* 256:615–46. doi: 10.1017/S0022112093002903.

Palakurthi, N. K. 2017. *Aerodynamics of particle detachment from surfaces: A numerical study*. MSc thesis, University of Cincinnati, Department of Mechanical & Materials Engineering.

Palakurthi, N. K., U. Ghia, and L. A. Turkevich. 2017. Simulation of particle detachment from a flat surface. Proc. ASME 2017 Fluids Eng. Div. Summer Meeting FEDSM2017-69111.

Palakurthi, N. K., U. Ghia, and L. A. Turkevich. 2022. Aerosolization of a particle on a hill: Numerical simulation of aerosolization in the Venturi dustiness tester. *J. Fluids Eng.* 144 (6):061113.

Patankar, N. A., and D. D. Joseph. 2001a. Modeling and numerical simulation of particulate flows by the Eulerian-Lagrangian approach. *Int. J. Multiphase Flow* 27 (10): 1659–84. doi: 10.1016/S0301-9322(01)00021-0.

Patankar, N. A., and D. D. Joseph. 2001b. Lagrangian numerical simulation of particulate flows. *Int. J. Multiphase Flow* 27 (10):1685–706. doi: 10.1016/S0301-9322(01)00025-8.

Pensis, I., J. Mareels, D. Dahmann, and D. Mark. 2010. Comparative evaluation of the dustiness of industrial minerals according to European standard EN 15051, 2006. *Ann. Occup. Hyg.* 54 (2):204–16. doi: 10.1093/annhyg/mep077.

Peters, T. M., S. Elzey, R. Johnson, H. Park, V. H. Grassian, T. Maher, and P. O'Shaughnessy. 2008. Airborne monitoring to distinguish engineered nanomaterials from incidental particles for environmental health and safety. *J. Occup. Environ. Health* 6 (2):73–81.

Plinke, M. A. E., D. Leith, M. G. Boundy, and F. Löffler. 1994. Dust generation from handling powders in industry. *Am. Ind. Hyg. J* 56 (3):251–7. doi: 10.1202/0002-8894(1995)056<0251:DGFHPI>2.0.CO;2.

Plinke, M. A. E., D. Leith, M. G. Boundy, and F. Löffler. 1995. Dust generation from handling powders in industry. *Am. Ind. Hyg. Assoc. J.* 56 (3):251–7. doi: 10.1202/0002-8894(1995)056<0251:DGFHPI>2.0.CO;2.

Plinke, M. A. E., D. Leith, R. G. Goodman, and F. Löffler. 1994. Particle separation mechanisms in flow of granular material. *Part. Sci. Technol.* 12 (1):71–87. doi: 10.1080/02726359408906642.

Plinke, M. A., D. Leith, D. B. Holstein, and M. G. Boundy. 1991. Experimental examination of factors that affect dust generation. *Am. Ind. Hyg. Assoc. J.* 52 (12):521–8. doi: 10.1080/15298669191365153.

Plinke, M. A., R. Maus, and D. Leith. 1992. Experimental examination of factors that affect dust generation by using Heubach and MRI testers. *Am. Ind. Hyg. Assoc. J.* 53 (5):325–30. doi: 10.1080/15298669291359726.

Powell, A. R., and C. C. Russell. 1933. Method for determining the dustiness of coal and coke. *Ind. Eng. Chem. Anal. Ed.* 5 (5):340–1. doi: 10.1021/ac50085a025.

Ren, H., and X.-Y. Lu. 2015. Dynamics and instability of a vortex ring impinging on a wall. *Commun. Comput. Phys.* 18 (4):1122–46. doi: 10.4208/cicp.150115.210715s.

Ren, H., G. X. Zhang, and H. S. Guan. 2016. Numerical study of the instability and flow transition in a vortex ring/wall interaction. *J. Appl. Fluid Mech.* 9 (7):2299–309. doi: 10.18869/acadpub.jafm.68.236.24926.

Ribalta, C., M. Viana, A. López-Lilao, S. Estupiñá, M. C. Minguillón, J. Mendoza, J. Díaz, D. Dahmann, and E. Monfort. 2019. On the relationship between exposure to particles and dustiness during handling of powders in industrial settings. *Ann. Work Expo. Health* 63 (1):107–23. doi: 10.1093/annweh/wxy092.

Saffman, P. G. 1965. The lift on a small sphere in a slow shear flow. *J. Fluid Mech.* 22 (2):385–400. doi: 10.1017/S0022112065000824.

Sallet, D. W. 1975. Impulsive motion of a circular disk which causes vortex rings. *Phys. Fluids* 18 (1):109–11. doi: 10.1063/1.860982.

Schiller, L., and A. Naumann. 1935. A drag coefficient correlation. *Zeits. Vereins Deutsches Ingenieure* 77:318–20.

Schulz, D., N. Schwindt, E. Schmidt, R. Jasevičius, and H. Kruggel-Emden. 2019. Investigation of the dust release from bulk material undergoing various processes using a coupled DEM/CFD approach. *Powder Technol.* 355:37–56. doi: 10.1016/j.powtec.2019.07.005.

Schwarzkopf, J., C. Crowe, and P. Dutta. 2009. Application of a volume averaged k-ε model to a particle-laden turbulent channel flow. *J. Fluid Eng.* 131 (10):101301.

Sharma, A. 2021. *Effect of vortex shedding on aerosolization of a particle from a hill using large Eddy simulation*. MSc thesis, University of Cincinnati, Department of Mechanical & Materials Engineering.

Sharma, A., U. Ghia, and L. A. Turkevich. 2020a. Effect of vortex shedding on the aerosolization of a particle from a hill using large Eddy simulation. Proc. 2020 AIAA Aviation Forum, 339120. doi: 10.2514/6.2020-2988.

Sharma, A., U. Ghia, and L. A. Turkevich. 2020b. Large Eddy simulation of flow over a hemispherical obstacle within a cylindrical tube. Proc. ASME 2020 Fluids Eng. Div. Summer Meeting FEDSM2020, 10596.

Shaw, B. W., P. P. Buharivala, C. B. Parnell Jr., and M. A. Denny. 1998. Emission factors for grain receiving and feed loading operations at feed mills. *Trans. ASAE* 41: 757–65.

Shenoy, A. R., and C. Kleinstreuer. 2008. Flow over a thin circular disk at low to moderate Reynolds numbers. *J. Fluid Mech.* 605:253–62. doi: 10.1017/S0022112008001626.

Shields, A. 1936. *Anwendung der Aehnlichkeitsmechanik und der Turbulenzforschung auf die Geschiebebewegung*. Vol. 26. Berlin: Mitteilungen der Preussischen Versuchsanstalt fur Wasserbau und Schiffbau [Translated by W. P. Ott and J. C. van Uchelen as 'Application of similarity principles and turbulence research to bed-load movement'].

Siemens Digital Industries Software. 2023. *STAR-CCM+*.

Snider, D. M., P. J. O'Rourke, and M. J. Andrews. 1998. Sediment flow in inclined vessels calculated using a multiphase particle-in-cell model for dense particle flows. *Int. J. Multiphase Flow* 24 (8):1359–82. doi: 10.1016/S0301-9322(98)00030-5.

Steiner, J., C. Morize, I. Delbende, A. Sauret, and P. Gondret. 2023. Vortex rings generated by a translating disk from start to stop. *Phys. Rev. Fluids* 8 (6):064702. doi: 10.1103/PhysRevFluids.8.064702.

Stokes, G. G. 1851. On the effect of internal friction on the motion of pendulums. *Trans. Camb. Philos. Soc.* 9:8–106.

Subramaniam, S. 2013. Lagrangian-Eulerian methods for multiphase flows. *Prog. Energy Combust. Sci.* 39 (2–3): 215–45. doi: 10.1016/j.pecs.2012.10.003.

Sutherland, A. J. 1967. Proposed mechanism for sediment entrainment by turbulent flow. *J. Geophys. Res.* 72 (24): 6183–94. doi: 10.1029/JZ072i024p06183.

Sutter, S. L., J. W. Johnston, and J. Mishima. 1982. Investigation of accident-generated aerosols: Releases from free-fall spills. *Am. Ind. Hyg. Assoc. J.* 43 (7):540–3. doi: 10.1080/15298668291410170.

Swearingen, J. D., J. D. Crouch, and R. A. Handler. 1995. Dynamics and stability of a vortex ring impacting a solid boundary. *J. Fluid Mech.* 297:1–28. doi: 10.1017/S0022112095002977.

Tartakovsky, A. M., K. F. Ferris, and P. Meakin. 2009. Lagrangian particle model for multiphase flows. *Comput. Phys. Commun.* 180 (10):1874–81. doi: 10.1016/j.cpc.2009.06.002.

Taylor, G. I. 1953. Formation of a vortex ring by giving an impulse to a circular disk and then dissolving it away. *J. Appl. Phys.* 24 (1):104. doi: 10.1063/1.1721114.

Trout, D. B., and P. A. Schulte. 2010. Medical surveillance and epidemiologic research for workers exposed to nanomaterials. *Toxicology* 269 (2–3):128–35. doi: 10.1016/j.tox.2009.12.006.

Tsuji, Y., Y. Morikawa, and H. Shiomi. 1984. LDV measurements of an air-solid two-phase flow in a vertical pipe. *J. Fluid Mech.* 139:417–34. doi: 10.1017/S0022112084000422.

Vincent, J. H., P. Baron, W. C. Hinds, W. John, G. Liden, M. Lippmann, M. A. McCawley, R. H. Phalen, R. S. Ratney, and B. O. Stuart. 1999. Particle size-selective sampling for particulate air contaminants. American Conference of Government Industrial Hygienists (ACGIH), Cincinnati OH, USA.

Walker, J. D. A., C. R. Smith, A. W. Cerra, and T. L. Doligalski. 1987. The impact of a vortex ring on a wall. *J. Fluid Mech.* 181 (1):99. doi: 10.1017/S0022112087002027.

Wells, A. B., and D. J. Alexander. 1978. A method for estimating the dust yield of powders. *Powder Technol.* 19 (2):271–7. doi: 10.1016/0032-5910(78)80036-9.

Wells, J. C. 1992. *Experiments on liquid-solid impact and particle pickup by impact of a vortex ring: applications to sediment transport*. PhD thesis, U. Grenoble I.

Wells, J. C., and E. J. Hopfinger. 1993. Visualization of particle pickup during vortex ring impact. Proc. 25th IAHR Congress (International Association for Hydraulic Research, Tokyo, 30 August–3 September 1993).

Xu, Y., and J. Wang. 2013. Recent developments of vortex ring impinging onto the wall. *Sci. China Technol. Sci.* 56 (10):2447–55. doi: 10.1007/s11431-013-5338-7.

Xu, Y., G. S. He, V. Kulkarni, and J. J. Wang. 2017. Experimental investigation of influence of Reynolds number on synthetic jet vortex rings impinging onto a solid wall. *Exp. Fluids* 58 (1):6. doi: 10.1007/s00348-016-2287-5.

Yang, A., L. Jia, and X. Yin. 2012. Formation process of the vortex ring generated by an impulsively started circular disc. *J. Fluid Mech.* 713:61–85. doi: 10.1017/jfm.2012.436.

Zhang, Y., and J. M. Reese. 2001. Particle-gas turbulence interactions in a kinetic theory approach to granular flows. *Int. J. Multiphase Flow* 27 (11):1945–64. doi: 10.1016/S0301-9322(01)00039-8.

Zhong, H. J., S. Y. Chen, and C. B. Lee. 2011. Experimental investigations of freely falling thin disks: Transition from zigzag to spiral. *Phys. Fluids* 23:011702.

Zhong, H., C. Lee, Z. Su, S. Chen, M. Zhou, and J. Wu. 2013. Experimental investigation of freely falling disks. Part 1: The flow structures and Reynolds number effects on the zigzag motion. *J. Fluid Mech.* 716:228–50. doi: 10.1017/jfm.2012.543.

Zhong, H.-J, and C.-B. Lee. 2012. The wake of falling disks at low Reynolds numbers. *Acta Mech. Sin.* 28 (2):367–71. doi: 10.1007/s10409-012-0036-4.

Zhou, C., J. Su, H. Chen, and Z. Shi. 2022. Terminal velocity and drag coefficient models for disc-shaped particles based on the imaging experiment. *Powder Technol.* 398:117062. doi: 10.1016/j.powtec.2021.117062.